Probing the Photoexcited States of Rhodium Corroles by Time-Resolved Q-Band EPR. Observation of Strong Spin−Orbit Coupling Effects

V. Rozenshtein,[†] L. Wagnert,[†] A. Berg,[†] E. Stavitski,[†,§] T. Berthold,[‡] G. Kothe,[‡] I. Saltsman,[#] Z. Gross,[#] and H. Levanon*,[†]

Department of Physical Chemistry, The Hebrew University of Jerusalem, Jerusalem 91904, Israel, Department of Physical Chemistry, University of Freiburg, Albertstrasse 21, D-79104 Freiburg, Germany, and Department of Chemistry and Institute of Catalysis Science and Technology, Technion - Israel Institute of Technology, Haifa 32000, Israel

Received: February 18, 2008; Revised Manuscript Received: March 31, 2008

The photoexcited states of two 5,10,15-tris(pentafluorophenyl)corroles (tpfc), hosting Rh(III) in their core, namely Rh(pyr)(PPh_3)(tpfc) and Rh(PPh_3)(tpfc), have been studied by time-resolved electron paramagnetic resonance (TREPR) combined with pulsed laser excitation. Using the transient nutation technique, the spin polarized spectra are assigned to photoexcited triplet states. The spectral widths observed for the two Rh(III) corroles crucially depend on the axial ligands at the Rh(III) metal ion. In case of Rh(PPh_3)(tpfc), the TREPR spectra are found to extend over 200 mT, which exceeds the spectral width of non-transition-metal corroles by more than a factor of 3. Moreover, the EPR lines of the Rh(III) corroles are less symmetric than those of the non-transition-metal corrroles. The peculiarities in the TREPR spectra of the Rh(III) corroles can be rationalized in terms of strong spin−orbit coupling (SOC) associated with the transition-metal character of the Rh(III) ion. It is assumed that SOC in the photoexcited Rh(III) corroles effectively admixes metal centered ^{3}dd-states to the corrole centered $^3\pi\pi^*$-states detected in the TREPR experiments. This admixture leads to an increased zero-field splitting and a large **g**-tensor anisotropy as manifested by the excited Rh(III) corroles.

Introduction

The development of a simple and efficient procedure for the synthesis of polypyrrolic macrocycles has initiated numerous studies of the chemical and physical properties of porphyrin analogues, such as the corroles.[1–12] However, in contrast to the metalloporphyrins,[13–16] the studies of the photoexcited states of metallocorroles are scarce.[17,18] As a matter of fact, direct studies of electronically excited corrole complexes involving transition-metal ions do not exist.

It is well-known that fully conjugated corrole or porphyrin rings each contain 18 delocalized π-electrons.[19,20] As a result, the corroles are structurally similar to the porhyrins but differ in the charge of the deprotonated macrocycle, which is −3 for corroles and −2 for porphyrins. Trianionic corrole macrocycles provide four pyrrole nitrogens as ligands for the central metal ion. Thus, two axial ligands can still be added. Generally, these axial ligands modify the energy of the metal centered states and can be used to "tune" the photochemical and photophysical properties of the transition-metal complex.[21] Although chemically and spectroscopically (in the UV−visible region) corroles are closely related to porphyrins,[22] the smaller cavity and reduced symmetry of the corroles (C_{2v} as compared to D_{4h}) lead to distinct photophysical properties, as will be shown in the following.

In this paper we present the first time-resolved electron paramagnetic resonance (TREPR) study of two newly synthesized metallocorroles involving Rh(III) as transition-metal ion. The ground states of these complexes are diamagnetic and, thus, EPR silent. Our objective is a detailed spectroscopic characterization of the photoexcited states of the Rh(III) corroles using TR Q-band (34 GHz) EPR combined with pulsed laser excitation. Particular emphasis is given to the exploration of the zero-field splitting (ZFS) observable in the TREPR spectra. The two studied Rh(III) corroles contain 5,10,15-tris(pentafluorophenyl) corrole (tpfc) as macrocycle and possess different axial ligands. Figure 1 shows the molecular structure of the complexes Rh(pyr)(PPh_3)(tpfc), **2**, and Rh(PPh_3)(tpfc), **3**, together with the structure of Sn(Cl)(tpfc), **1**, included in the study for comparison. The specific choice of these metallocorroles allows for the identification of strong spin−orbit coupling (SOC) effects which can be related to the transition-metal character of the Rh(III) ion.

Materials and Methods

Sample Preparation. The two Rh(III) corroles, Rh(pyr)(PPh_3)(tpfc) and Rh(PPh_3)(tpfc) (see Figure 1), coordinated by different axial ligands, were synthesized as described elsewhere.[23,24] The EPR spectroscopic properties of the Sn(IV) corrole, namely, Sn(Cl)(tpfc) (see Figure 1), have been published earlier.[17] The Rh(III) complexes were dissolved in the liquid crystal (LC) E-7 (Merck Ltd.). The concentrations used were $\sim 5 \times 10^{-4}$ mol/L. The LC E-7 was used without further purification. The Rh(III) corroles were first dissolved in toluene, which was then evaporated and the LC was introduced into the quartz tube. The samples were degassed by several freeze−pump−thaw cycles on a vacuum line and sealed under vacuum.[17]

The LC E-7 shows a clearing temperature of 333 K and a melting point of 263 K. In general, however, E-7 avoids crystallization and, thus, exhibits a nematic phase between 333 K and the melting point and a "nematic glass" below 263 K, which was found to be stable down to very low temperatures.

* Corresponding author. E-mail: levanon@chem.ch.huji.ac.il.
[†] The Hebrew University of Jerusalem.
[§] Current address: Inorganic Chemistry and Catalysis Group, Utrecht University, Sorbonnelaan 16, 3584 CA Utrecht, The Netherlands.
[‡] University of Freiburg.
[#] Technion - Israel Institute of Technology.

10.1021/jp801425d CCC: $40.75
Published on Web 05/29/2008

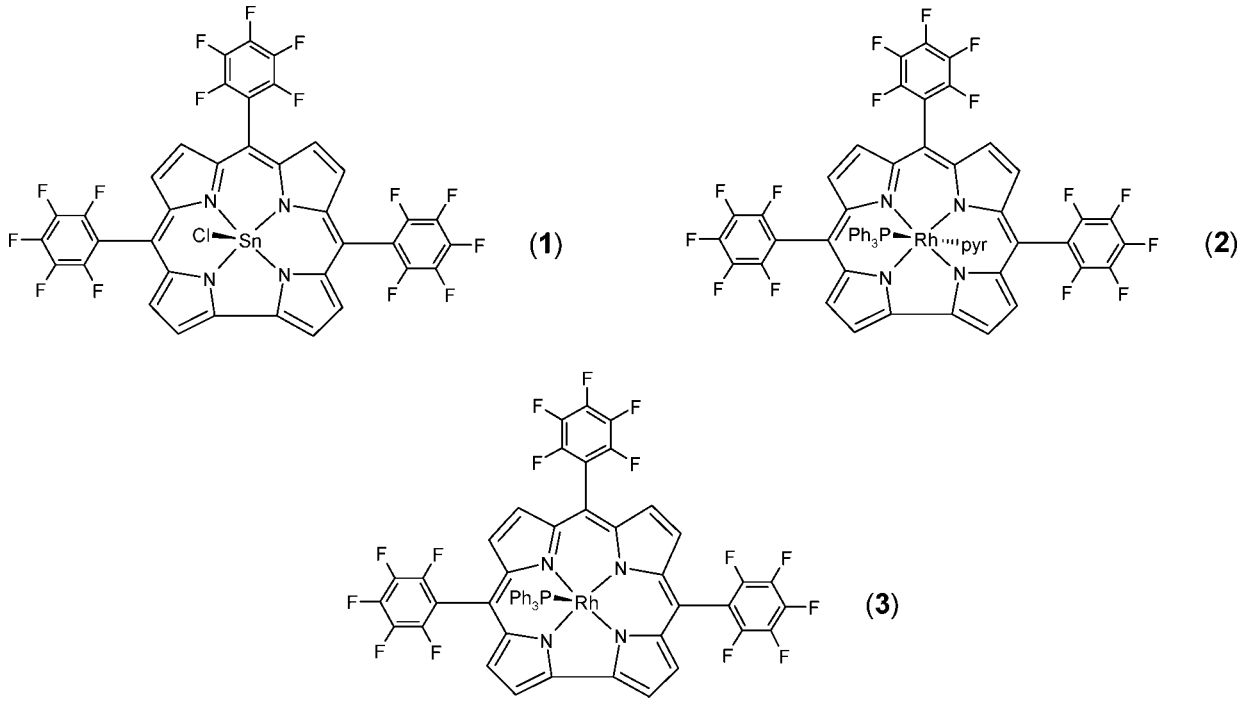

Figure 1. Molecular structures of the studied metallocorroles: Sn(Cl)(tpfc), **1**; Rh(pyr)(PPh_3)(tpfc), **2**; Rh(PPh_3)(tpfc), **3**.

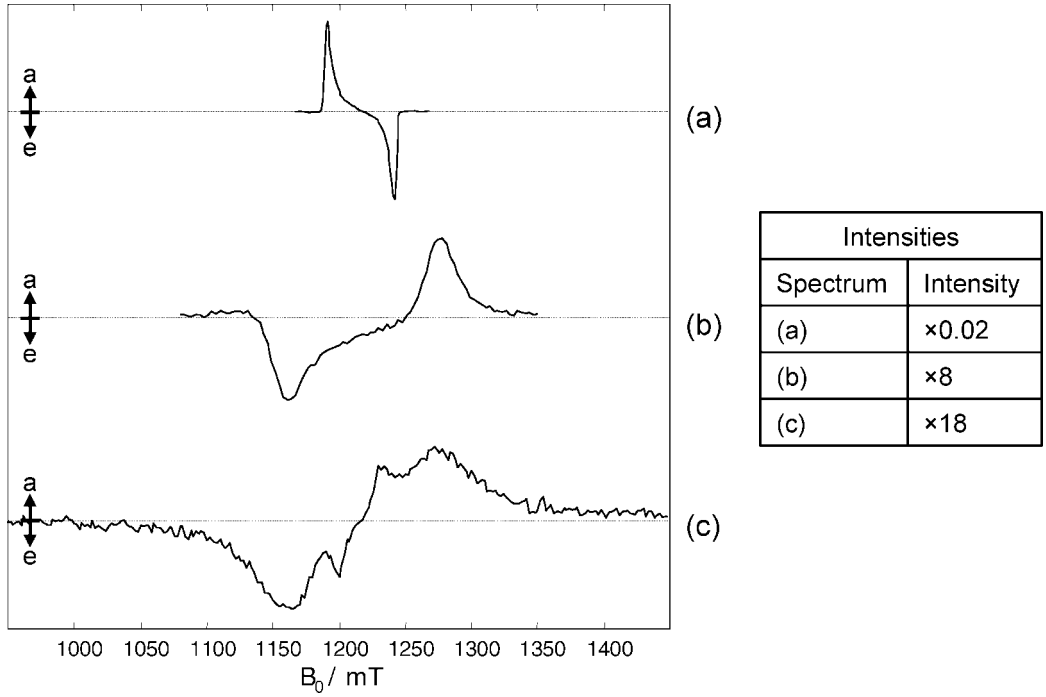

Figure 2. Time-resolved Q-band EPR spectra (χ'' representation) of various photoexcited metallocorroles in the liquid crystal E-7 at parallel orientation of director and magnetic field (**L** || **B**). Positive and negative signals indicate absorptive (a) and emissive (e) electron spin polarization, respectively. The EPR spectra were taken 150 ns after laser pulse excitation at 100 K. (a) Tin corrole, Sn(Cl)(tpfc), **1**. (b) Rhodium corrole, Rh(pyr)(PPh_3)(tpfc), **2**. (c) Rhodium corrole, Rh(PPh_3)(tpfc) **3**.

The orientation of the LC director, **L**, with respect to the magnetic field, **B**, is determined by the sign of the anisotropy of the diamagnetic susceptibility. Because for E-7 the sign is positive, the director aligns parallel to the magnetic field, i.e., **L**||**B**. Rotating the frozen sample by 90° about an axis perpendicular to the magnetic field yields the director orientation **L** ⊥ **B**.

EPR Measurements. The TREPR measurements were performed with a transient Q-band (34 GHz) bridge (Bruker ER 050 QGT) in combination with a Bruker ESP 300E console. The quartz sample tube (i.d. 2 mm) was irradiated in a cylindrical cavity with a loaded Q of approximately 700, which corresponds to a bandwidth of 50 MHz. A transient recorder (LeCroy 9354A) with a digitizing rate of 1 ns/11 bit sample was used to acquire the time dependent EPR signal. The time resolution of the experimental setup is in the 10 ns range. Typically, 100 transients were accumulated to improve the signal/noise ratio. A weak laser-induced cavity signal was eliminated by substracting transients accumulated at off-resonance conditions.[25] The sample temperature was regulated by an

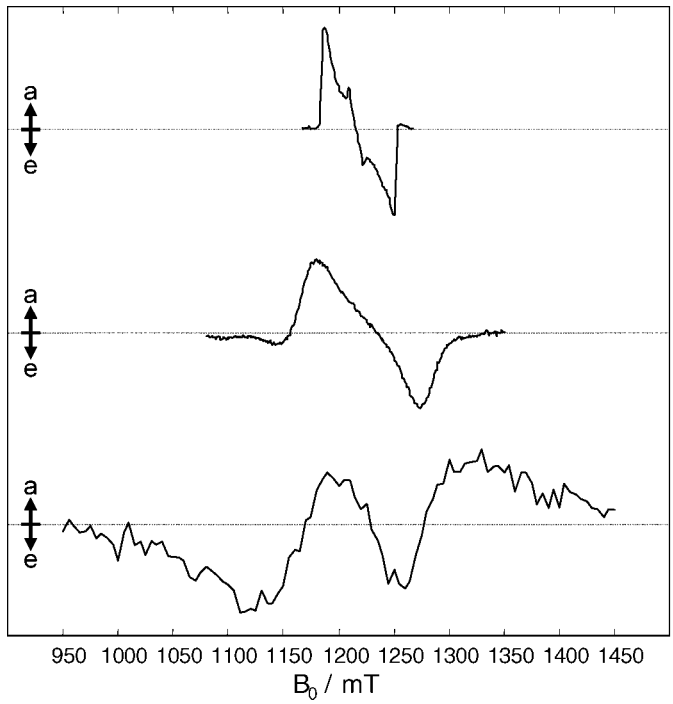

Intensities	
Spectrum	Intensity
(a)	×0.015
(b)	×1
(c)	×10

Figure 3. Time-resolved Q-band EPR spectra (χ'' representation) of various photoexcited metallocorroles in the liquid crystal E-7 at perpendicular orientation of director and magnetic field ($\mathbf{L} \perp \mathbf{B}$). Positive and negative signals indicate absorptive (a) and emissive (e) electron spin polarization, respectively. The EPR spectra were taken 150 ns after laser pulse excitation at 100 K. (a) Tin corrole, Sn(Cl)(tpfc), **1**. (b) Rhodium corrole, Rh(pyr)(PPh_3)(tpfc), **2**. (c) Rhodium corrole, Rh(PPh_3)(tpfc) **3**.

Oxford temperature controller (model ITC 503) coupled to an Oxford helium flow cryostat (Oxford CF-935).

Optical excitation was carried out with an OPO system (OPTA GmbH), pumped by a Nd:YAG laser (Spectra Physics Quanta Ray GCR 190-10). The excitation wavelength was selected according to the low-energy absorption Q-band of the Rh(III) corroles ranging from 580 to 596 nm. In all experiments a pulse width of 2.5 ns and a laser repetition rate of 10 Hz were used. Generally, the laser intensity was attenuated to ~3 mJ/pulse. To avoid photoselection, the laser beam was passed through a quartz depolarizer.

Results and Discussion

Transient EPR Spectra. Generally, a complete data set of a TREPR experiment consists of transient signals taken at equidistant field points covering the total spectral width. This yields a two-dimensional variation of the signal intensity with respect to both the magnetic field and the time axes.[26] Transient spectra can be extracted from such a plot at any time after the laser pulse as slices parallel to the magnetic field axis. Likewise, the time evolution of the transverse magnetization may be obtained for any given field as a slice along the time axis.

Typical Q-band (34 GHz) EPR spectra of the photoexcited Rh(III) corroles, **2** and **3** and the Sn(IV) corrole **1**, detected 150 ns after the laser pulse, are shown in the Figures 2 and 3. The line shapes are characteristic of triplet states[27–32] or higher multiplet spin states with large dipolar interactions between the unpaired electron spins. Notably, the spectral widths observed for the two Rh(III) corroles crucially depend on the axial ligands at the transition-metal ion. Closer inspection reveals that the TREPR spectra of **3** extend over 200 mT and thus exceed the spectral width of **1** and other non-transition-metal corroles[17,33] by more than a factor of 3.

All TREPR spectra refer to the same temperature ($T = 100$ K) but reflect different orientational distributions of the metallocorroles **1**−**3** with respect to the laboratory frame. A spin polarization effect is observed for all partially ordered samples.[27–32] This is not surprising as the selectivity in the population of the zero-field spin states can be detected by this method before relaxation sets in. Generally, a positive signal indicates absorptive (a) and a negative emissive (e) spin polarization.

The TREPR spectra of Figure 2 show the electron spin polarization for anisotropic distributions of **1**−**3** with the LC director parallel to the magnetic field ($\mathbf{L} \parallel \mathbf{B}$). The spectra of Figure 3 refer to partially ordered samples with the director perpendicular to the magnetic field ($\mathbf{L} \perp \mathbf{B}$). Substantial spectral differences are observed when the sample is rotated.

Inspection of the TREPR spectra reveals that the line shapes can be characterized by a spin Hamiltonian, which accounts for anisotropic electron Zeeman and dipolar interactions

$$H = H_Z + H_{ZFS} = \beta \mathbf{B}\cdot\mathbf{g}\cdot\mathbf{S} + \mathbf{S}\cdot\mathbf{D}\cdot\mathbf{S} \qquad (1)$$

Here, β is the Bohr magneton, **B** is the external magnetic field, **g** is the **g**-tensor of the paramagnetic species, **S** is the total electron spin operator and **D** is the ZFS tensor. In the principal axis system of the ZFS tensor, the dipolar term can be written as

$$H_{ZFS} = D_{XX}S_X^2 + D_{YY}S_Y^2 + D_{ZZ}S_Z^2 = D\left[S_Z^2 - \frac{1}{3}S(S+1)\right] + E(S_X^2 - S_Y^2), \qquad (2)$$

where $D = {}^3/_2 D_{ZZ}$ and $E = {}^1/_2(D_{XX} - D_{YY})$ are the ZFS parameters of the paramagnetic species. If we assume, for simplicity, that the ZFS tensor and the **g**-tensor are collinear, the Zeeman term of the spin Hamiltonian can be expanded in the principal axis system of the ZFS tensor according to

$$H_Z = \beta(B_X g_{XX} S_X + B_Y g_{YY} S_Y + B_Z g_{ZZ} S_Z) \quad (3a)$$

$$g = \frac{1}{3}(g_{XX} + g_{YY} + g_{ZZ}) \quad (3b)$$

Here B_i is the ith component of **B** in the dipolar tensor frame, g_{XX}, g_{YY} and g_{ZZ} are the principal values of the **g**-tensor and g denotes the isotropic g-factor defined in eq 3b.

Thus, a detailed analysis of the spin polarized EPR spectra can provide the ZFS parameters, D, E, and the **g**-tensor components g_{XX}, g_{YY}, and g_{ZZ} of the two photoexcited Rh(III) corroles. If the ZFS tensor and the **g**-tensor are not collinear, three more parameters (Euler angles) are required to specify the mutual orientation of the two magnetic tensors. Clearly, such a large number of magnetic parameters may only be evaluated by a complete spectral simulation of the spin polarized EPR spectra. Notably, these simulations can also yield the populations of the zero-field sublevels, which determine the electron spin polarization in the high-field EPR spectra.[27–32] Finally, detailed analysis of the angular dependent line shapes can provide values for the order parameters of the Rh(III) corroles in the LC as well as information on the mutual orientation of the ZFS and order tensor.[27–32]

Transient Nutations. The transient nutation experiments were carried out to identify the paramagnetic species responsible for the observed TREPR spectra. Generally, this technique provides information on the spin quantum number of the detected paramagnetic state and on the spin projections which characterize the Zeeman sublevels participating in the transition.[34–37] Figure 4 shows the time evolution of the transverse magnetization for the photoexcited Rh(III) corroles **2** and **3,** measured at the fields of maximum absorptive signal in the "parallel" (**L** || **B**) TREPR spectra. The transients refer to a microwave field of $B_1 = 0.025$ mT and a common temperature of $T = 30$ K. Evidently, both time profiles exhibit transient nutations whose frequency ω_N can be determined by Fourier transformation. The result is shown in the insets of Figure 4. One observes a single frequency peak at $\omega_N/2\pi \approx 1.07$ MHz. Similar results were obtained for measurements at various other field positions both in the "parallel" (**L** || **B**) and in the "perpendicular" (**L** ⊥ **B**) EPR spectra (not shown).

Analyzing the nutation frequency according to

$$\omega_N = [S(S+1) - M_S(M_S - 1)]^{1/2}\omega_1 \quad (4a)$$

$$\omega_1 = (g\beta/\hbar)B_1 \quad (4b)$$

provides an easy means for determining the electron spin quantum number of the paramagnetic state.[37,38] The relation (4) is valid when the transition $|S,M_S-1\rangle \rightarrow |S,M_S\rangle$ is excited selectively by microwaves.[39] The ground states of the two Rh(III) corroles are electronic singlets. Thus, the photoexcited states of **2** and **3**, which give rise to the observed TREPR spectra, can either be a triplet or a quintet. Equation 4 predicts a single nutation frequency of $(\omega_N)_T = 2^{1/2}\,\omega_1$ for a photoexcited triplet state. In contrast, there should be two different nutation frequencies of $(\omega_N)_Q = 2\,\omega_1$ and $(\omega_N)_Q = 6^{1/2}\,\omega_1$ in case of an excited quintet state.

Our nutation experiment always indicate a single frequency peak at $\omega_N/2\pi \approx 1.07$ MHz, independent of the selected field position in the TREPR spectra. For a triplet state and $B_1 = 0.025$ mT, one expects a nutation frequency of $(\omega_N/2\pi)_{calc} = 1.0$ MHz, in excellent agreement with the experimental findings. Thus, we assign the photoexcited states of **2** and **3** to electronic triplets.

In principle, these triplet states may originate either from π-electron transitions of the corrole macrocycle or from d-electron transitions of the Rh(III) transition-metal ion. In the latter case, one would expect ZFS parameters of the order of $D \sim 1$ cm^{-1},[40] which is not observed experimentally. We therefore

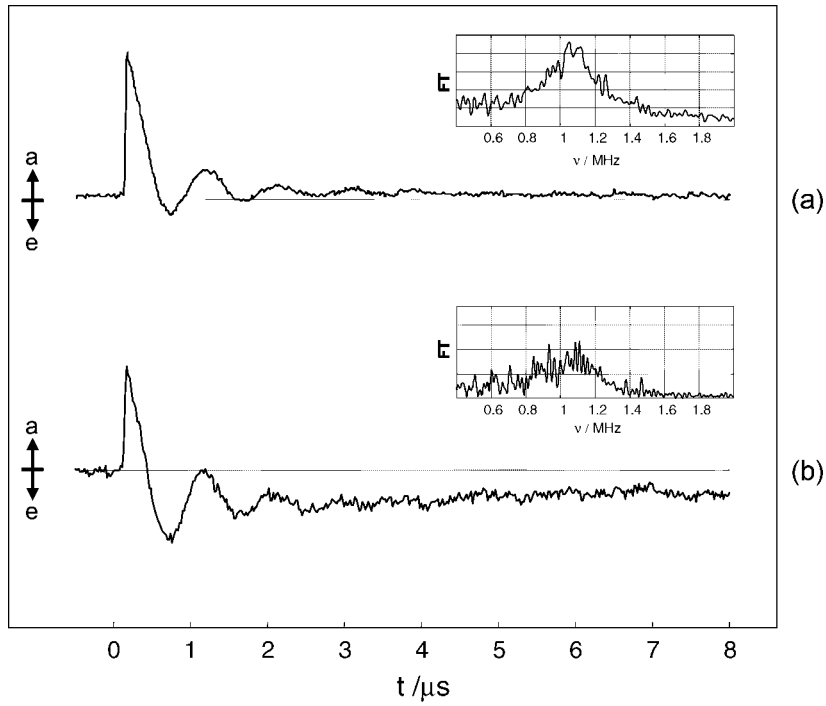

Figure 4. Time evolution of the transverse Q-band magnetization of two photoexcited Rh(III) corroles in the liquid crystal E-7. Positive and negative signals indicate absorptive (a) and emissive (e) electron spin polarization, respectively. The transients were measured at the fields of maximum absorptive signal in the "parallel" (**L** || **B**) TREPR spectra (see Figure 2) and refer to a common temperature of 30 K. Microwave power: $B_1 = 0.025$ mT. (a) Rh(pyr)(PPh_3)(tpfc) taken at 1270 mT, **2**. (b) Rh(PPh_3)(tpfc) taken at 1230 mT, **3**. The Fourier transform (FT) of the time profiles is shown in the insets.

believe that the observed TREPR spectra are basically due to $\pi\pi^*$ triplet states of the corrole macrocycle.

Spin−Orbit Coupling. In the Figures 2 and 3 we compare the TR Q-band EPR spectra of the photoexcited Rh(III) corroles **2** and **3** with those of the non-transition-metal corrole Sn(Cl)(tpfc), **1**.[17] The spectra refer to the same temperature ($T = 100$ K) but different orientational distributions of the metallocorroles embedded in the LC E-7. The spin polarized EPR spectra of Figure 2 reflect anisotropic molecular distributions in which the director of the LC is parallel to the magnetic field (**L** || **B**). In the EPR spectra of Figure 3, the director is oriented perpendicular to the magnetic field (**L** ⊥ **B**).

Two major differences are observed in the TREPR spectra obtained either from the transition-metal corroles **2** and **3** or from the non-transition-metal corrole **1**. First, the spin polarized EPR spectra of the Rh(III) corroles are much broader than those of the Sn(IV) corrole and exhibit a distinct polarization pattern. Notably, the increased spectral width observed for the Rh(III) corroles depends on the axial ligands at the transition-metal ion. Second, the EPR line shapes of the Rh(III) corroles are less symmetric than those of the Sn(IV) corrole. This spectral asymmetry is more pronounced in the "perpendicular" EPR spectra shown in Figure 3.

How can we rationalize these peculiarities in the TREPR spectra of the photoexcited Rh(III) corroles? One plausible explanation are strong SOC effects associated with the transition-metal character of the Rh(III) ion. We believe that SOC in the Rh(III) corroles effectively admixes metal centered ^{3}dd-states to the corrole centered $^3\pi\pi^*$-state detected in the TREPR experiments. This admixture leads to an increased ZFS and a large **g**-tensor anisotropy not observed for non-transition-metal corroles.[17,33] Although the SOC constants of Rh and Sn are similar, Sn(IV) possesses a filled d-shell and thus has no metal centered ^{3}dd-states near the detected $^3\pi\pi^*$-state of the corrole macrocycle. We believe that this is the main reason for the negligibly small SOC effects observed in the TREPR spectra of Sn(IV) corrole and other non-transition-metal corroles.[17,33]

Zero-Field Splitting. For simplicity, we discuss SOC effects on the ZFS only for the larger ZFS parameter D. It can be shown that this parameter, defined in eq 2, comprises two different contributions

$$D = D_{SS} + D_{SOC} \tag{5}$$

where D_{SS} is due to magnetic dipolar interactions between the unpaired electron spins and D_{SOC} originates from SOC in the photoexcited metallocorroles. For Sn(IV) corrole, a ZFS parameter of $D(\mathbf{1}) \approx -0.03$ cm^{-1} was reported.[17] Because SOC effects in non-transition-metal corroles are small, we can assess $D_{SS}(\mathbf{1}) \approx D(\mathbf{1}) \approx -0.03$ cm^{-1}. Taking the overall splitting of the "perpendicular" EPR spectra (see Figure 3) as a measure of $2D$, we can estimate the ZFS parameters of the Rh(III) corroles by $D(\mathbf{2}) \approx 0.06$ cm^{-1} and $D(\mathbf{3}) \approx 0.1$ cm^{-1}. The positive sign of D is suggested by the sign reversal of the electron spin polarization upon substitution of Rh(III) for Sn(IV) (see Figure 2). Assuming further that D_{SS} of the Rh(III) corroles is approximately equal to D_{SS} of the Sn(IV) corrole, we finally obtain $D_{SOC}(\mathbf{2}) \approx 0.09$ cm^{-1}and $D_{SOC}(\mathbf{3}) \approx 0.13$ cm^{-1} (see eq 5). Note that these large SOC contributions significantly vary with the axial ligands at the Rh(III) ion, which modify the energy of the metal centered ^{3}dd-states.

g-Tensor Anisotropy. For non-transition-metal corroles such as Ga(III) corrole and Sn(IV) corrole, the assumption of an isotropic **g**-tensor

$$g_{XX} = g_{YY} = g_{ZZ} = g \tag{6}$$

is a reasonable approximation that considerably simplifies the analysis of the TREPR spectra.[17,33] However, in the case of the Rh(III) corroles this approximation cannot be used anymore. Here, strong SOC effects lead to asymmetric line shapes already in Q-band EPR. This is clearly seen in Figure 3, depicting the "perpendicular" EPR spectra of the metallocorroles. In these spectra, the signal maxima and minima can be shifted from their "canonical" positions. Thus, it is generally not possible to extract meaningful values for D, E, g_{XX}, g_{YY} and g_{ZZ} without a detailed spectral simulation.

If we assume that the orientational distribution of the metallocorroles about the LC director **L** is rather narrow, then for **L** || **B** one of the three magnetic field projections is much larger than the other two. This means that the expansion of the Zeeman Hamiltonian in eq 3a reduces to one term. As a result, the "parallel" EPR spectra can effectively be described by a single g-value. This might be the reason why the "parallel" EPR spectra of **1** and the transition-metal corroles **2** and **3** look very similar, indicating line shapes with isotropic g-values (see Figure 2). However, in the "perpendicular" EPR spectra, the two other magnetic field projections are expected to be much larger than the first one. Thus, the g-values are smeared out over a large magnetic field range and, as a result, peaks from different "canonical" orientations may overlap. If these peaks have opposite polarizations, the overall EPR line shape becomes unexpectedly complex and a straightforward analysis is impaired.

Conclusions

We have shown that the TREPR spectra of two photoexcited metallocorroles, hosting Rh(III) in their core, are significantly different from those of non-transition-metal corroles.

The observed enhanced ZFS and the large **g**-tensor anisotropy can be rationalized in terms of strong SOC associated with the transition-metal character of the Rh(III) ion. It is demonstrated that SOC in the photoexcited Rh(III) corroles effectively admixes metal centered ^{3}dd-states to the corrole centered $^3\pi\pi^*$-states detected in the TREPR experiments. The efficiency of this admixture depends on the number and type of axial ligands at the Rh(III) transition-metal ion.

Acknowledgment. Work at the Hebrew University of Jerusalem (HUJ) was supported by the Israel Science Foundation (grant number 740/06), the Humboldt Foundation (H.L.), and the KAMEA Foundation (V.R. and A.B.). Work at Technion was supported by the Israel Science Foundation (grant number 740/06) and a Technion VPR fund (Z.G.). The center for absorption in Science, Ministry of Immigration is also acknowledged (I.S.). This work is in partial fulfillment of the requirements for a Ph.D. degree (L.W.) at the Hebrew University of Jerusalem. We are thankful to Mr. R. Rubin for this help in editing the text and figures.

References and Notes

(1) Gross, Z.; Galili, N.; Saltsman, I. *Angew. Chem., Int. Ed. Engl.* **1999**, *38*, 1427.
(2) Mahammed, A.; Gross, Z. *J. Inorg. Biochem.* **2002**, *88*, 305.
(3) Paolesse, R.; Jaquinod, L.; Nurco, D. J.; Mini, S.; Sagone, F.; Boschi, T.; Smith, K. M. *Chem. Commun.* **1999**, *14*, 1307.
(4) Gross, Z.; Galili, N.; Simkhovich, L.; Saltsman, I.; Botoshansky, M.; Blaser, D.; Boese, R.; Goldberg, I. *Org. Lett.* **1999**, *1*, 599.
(5) Gryko, D. T. *Eur. J. Org. Chem.* **2002**, 1735.
(6) Nardis, S.; Monti, D.; Paolesse, R. *Mini-Rev. Org. Chem.* **2005**, *2*, 355.
(7) Gross, Z.; Gray, H. B. *Adv. Synth. Catal.* **2004**, *346*, 165.

(8) Gryko, D. T.; Fox, J. P.; Goldberg, D. P. *J. Porphyrins Phthalocyanines* **2004**, *8*, 1091.
(9) Aviv, I.; Gross, Z. *Chem. Commun.* **2007**, *20*, 1987.
(10) Goldberg, D. P. *Acc. Chem. Res.* **2007**, *40*, 626.
(11) Fu, B. Q.; Huang, J.; Ren, L.; Weng, X. C.; Zhou, Y. Y.; Du, Y. H.; Wu, X. J.; Zhou, X.; Yang, G. F. *Chem. Commun.* **2007**, 3264.
(12) Weaver, J. J. Corroles. Ph.D. Thesis, California Institute of Technology, Pasadena, 2005.
(13) Lomova, T. N.; Berezin, B. D. *Russ. J. Coord. Chem.* **2001**, *27*, 85.
(14) Van der Waals, J. H.; Van Dorp, W. G.; Schaafsma, T. J. ESR of Porphyrin Excited States. In *The Porphyrins*; Dolphin, D. , Ed.; Academic Press: New York, 1979; Vol. 4, Part B, p 257.
(15) Canters, G. W.; van der Waals, J. H. High-Resolution Zeeman Spectroscopy of Metalloporphyrins. In *The Porphyrins*; Dolphin, D., Ed.; Academic Press Inc.: New York, 1978; Vol. III; p 531.
(16) Gouterman, M. Optical Spectra and Electronic Structure of Porphyrins and Related Rings. In *The Pophyrins*; Dolphin, D., Ed.; Academic Press: New York, 1978; Vol. 3, p 1.
(17) Wagnert, L.; Berg, A.; Stavitski, E.; Berthold, T.; Kothe, G.; Goldberg, I.; Mahammed, A.; Simkhovich, L.; Gross, Z.; Levanon, H. *Appl. Magn. Reson.* **2006**, *30*, 591.
(18) Wagnert, L.; Berg, A.; Stavitski, E.; Luobeznova, I.; Gross, Z.; Levanon, H. *J. Porphyrins Phthalocyanines* **2007**, *11*, 645.
(19) Paolesse, R. Syntheses of Corroles. In *The Porphyrin Handbook*; Kadish, K. M., Smith, K. M., Guilard, R., Eds.; Academic Press: New York, 2000; Vol. 2, p 201.
(20) Bruckner, C.; Barta, C. A.; Brinas, R. P.; Bauer, J. A. K. *Inorg. Chem.* **2003**, *42*, 1673.
(21) Ford, P. C.; Wink, D.; Dibenedetto, J. *Prog. Inorg. Chem.* **1983**, *30*, 213.
(22) Erben, C.; Will, S.; Kadish, K. M. Metallocorroles: Molecular Structure, Spectroscopy and Electronic States. In *The Porphyrin Handbook*; Kadish, K. M., Smith, K. M., Guilard, R., Eds.; Academic Press: New York, 2000; Vol. 2, p 233.
(23) Simkhovich, L.; Galili, N.; Saltsman, I.; Goldberg, I.; Gross, Z. *Inorg. Chem.* **2000**, *39*, 2704.
(24) Simkhovich, L.; Goldberg, I.; Gross, Z. *J. Porphyrins Phthalocyanines* **2002**, *6*, 439.
(25) Heinen, U.; Berthold, T.; Kothe, G.; Stavitski, E.; Galili, T.; Levanon, H.; Wiederrecht, G.; Wasielewski, M. R. *J. Phys. Chem. A* **2002**, *106*, 1933.
(26) Stehlik, D.; Bock, C. H.; Turnauer, M. C. *Transient EPR Spectroscopy of Photoinduced Electronic Spin States in Rigid Matrices In Advanced EPR*; Hoff, A. J., Ed.; Elsevier: Amsterdam, 1989; *Vol. Chapter 11*; p. 371.
(27) Regev, A.; Galili, T.; Levanon, H. *J. Chem. Phys.* **1991**, *95*, 7907.
(28) Gonen, O.; Levanon, H. *J. Phys. Chem.* **1984**, *88*, 4223.
(29) Levanon, H. *Rev. Chem. Intermed.* **1987**, *8*, 287.
(30) Fessmann, J.; Rosch, N.; Ohmes, E.; Kothe, G. *Chem. Phys. Lett.* **1988**, *152*, 491.
(31) Munzenmaier, A.; Rosch, N.; Weber, S.; Feller, C.; Ohmes, E.; Kothe, G. *J. Phys. Chem.* **1992**, *96*, 10645.
(32) Gamliel, D.; Levanon, H. *J. Chem. Phys.* **1992**, *97*, 7140.
(33) Stavitski, E.; Berg, A.; Ganguly, T.; Mahammed, A.; Gross, Z.; Levanon, H. *J. Am. Chem. Soc.* **2004**, *126*, 6886.
(34) Torrey, H. *Phys. Rev.* **1949**, *76*, 1059.
(35) Kim, S. S.; Weissman, S. I. *Rev. Chem. Intermed.* **1979**, *3*, 107.
(36) Furrer, R.; Fujara, F.; Lange, C.; Stehlik, D.; Vieth, H. M.; Vollmann, W. *Chem. Phys. Lett.* **1980**, *75*, 332.
(37) Astashkin, A. V.; Schweiger, A. *Chem. Phys. Lett.* **1990**, *174*, 595.
(38) Mizuochi, N.; Ohba, Y.; Yamauchi, S. *J. Phys. Chem. A* **1997**, *101*, 5966.
(39) Abragam, A. *The Principles of Nuclear Magnetism*; Clarendon Press: Oxford, U.K., 1961.
(40) Boca, R. *Coord. Chem. Rev.* **2004**, *248*, 757.

JP801425D